

Search for light dark matter with NEWS-G at the LSM using a methane target

M. M. Arora,¹ L. Balogh,¹ C. Beaufort,² A. Brossard,^{3,*} M. Chapellier,³ J. Clarke,³ E. C. Corcoran,⁴ J.-M. Coquillat,^{3,†} A. Dastgheibi-Fard,² Y. Deng,⁵ D. Durnford,^{5,‡} C. Garrah,⁵ G. Gerbier,³ I. Giomataris,⁶ G. Giroux,³ P. Gorel,⁷ M. Gros,⁶ P. Gros,³ O. Guillaudin,⁸ E. W. Hoppe,⁹ I. Katsioulas,^{10,§} F. Kelly,⁴ P. Knights,¹⁰ P. Lautridou,¹¹ A. Makowski,³ I. Manthos,^{10,12} R. D. Martin,³ J. Matthews,¹⁰ H. M. McCallum,⁴ H. Meadows,³ L. Millins,¹⁰ J.-F. Muraz,² T. Neep,¹⁰ K. Nikolopoulos,^{10,12} N. Panchal,³ M.-C. Piro,⁵ N. Rowe,³ D. Santos,² G. Savvidis,³ I. Savvidis,¹³ D. Spathara,¹⁰ F. Vazquez de Sola Fernandez,^{11,¶} and R. Ward^{10,12}

(NEWS-G Collaboration)

¹*Department of Mechanical and Materials Engineering,
Queen's University, Kingston, Ontario K7L 3N6, Canada*

²*LPSC-LSM, Université Grenoble-Alpes, CNRS-IN2P3, Grenoble, 38026, France*

³*Department of Physics, Engineering Physics & Astronomy,
Queen's University, Kingston, Ontario, K7L 3N6, Canada*

⁴*Chemistry & Chemical Engineering Department,
Royal Military College of Canada, Kingston, Ontario K7K 7B4, Canada*

⁵*Department of Physics, University of Alberta, Edmonton, T6G 2E1, Canada*

⁶*IRFU, CEA, Université Paris-Saclay, F-91191 Gif-sur-Yvette, France*

⁷*SNOLAB, Lively, Ontario, P3Y 1N2, Canada*

⁸*LPSC, Université Grenoble-Alpes, CNRS-IN2P3, Grenoble, 38026, France*

⁹*Pacific Northwest National Laboratory, Richland, Washington 99354, USA*

¹⁰*School of Physics and Astronomy, University of Birmingham, Birmingham, B15 2TT, UK*

¹¹*SUBATECH, IMT-Atlantique/CNRS-IN2P3/Nantes University, Nantes, 44307, France*

¹²*Institute for Experimental Physics, University of Hamburg, Hamburg, 22767, Germany*

¹³*Aristotle University of Thessaloniki, Thessaloniki, 54124 Greece*

(Dated: July 18, 2024)

The NEWS-G direct detection experiment uses spherical proportional counters to search for light dark matter candidates. New results from a 10 day physics run with a 135 cm in diameter spherical proportional counter at the Laboratoire Souterrain de Modane are reported. The target consists of 114 g of methane, providing sensitivity to dark matter spin-dependent coupling to protons. New constraints are presented in the mass range 0.17 to 1.2 GeV/c², with a 90% confidence level cross-section upper limit of 30.9 pb for a mass of 0.76 GeV/c².

Astronomical and cosmological observations strongly suggest the existence of non-baryonic dark matter (DM) in our universe [1, 2]. Theories beyond the Standard Model provide DM candidates in the form of non-relativistic, weakly interacting, massive particles (WIMPs) [3, 4] constituting our galactic halo. The NEWS-G experiment employs spherical proportional counters (SPCs) filled with various gases to search for WIMP-like particles scattering off target nuclei, producing nuclear recoil energies of up to several keV. First constraints using this technology were obtained with a 60 cm in diameter SPC filled with a neon and methane mixture [5].

The new S140 detector [6] consists of a grounded 135 cm in diameter SPC constructed with low background Oxygen-Free High-Conductivity copper (C10100) featur-

ing a 0.5 mm inner shield made of high-purity electroformed copper [7]. It is equipped [6] with a multi-anode sensor, “ACHINOS” [8, 9], developed to ensure both primary charge collection and high charge amplification capabilities. It is held at the center of the SPC with a support rod, also used to apply a high voltage on the anodes, and from which the signal is read out. The 11 anodes are grouped into two readout channels: one comprising the five nearest anodes to the support rod (“Near” anodes) and the other with the six farthest (“Far” anodes). A UV laser system and a gaseous ³⁷Ar radioactive source provide *in situ* calibration to characterize and monitor the detector response.

This letter reports new DM results based on data taken during the commissioning of this detector at the Laboratoire Souterrain de Modane (LSM), before its installation at SNOLAB. The SPC was filled with 135 mbar of methane and operated with a water shield for approximately 10 days, for a total exposure of 1.12 kg · day. This hydrogen-rich target makes the experiment particularly sensitive to WIMP-like DM candidates with $\mathcal{O}(1 \text{ GeV}/c^2)$ masses, giving access to spin-dependent (SD) DM-proton couplings. This region is favoured by recent theoretical models [10–13].

After an energy deposition within the SPC, ionization

* now at TRIUMF, Vancouver, BC V6T 2A3, Canada

† e-mail: jeanmarie.coquillat@queensu.ca

‡ e-mail: ddurnfor@ualberta.ca

§ now at European Spallation Source ESS ERIC (ESS), Lund, SE-221 00, Sweden

¶ e-mail: 14favd@queensu.ca; now at Nikhef (Nationaal instituut voor subatomaire fysica)

electrons drift towards the anodes, where they are multiplied by an avalanche process close to the anode. The measured signal from a single primary electron reaching the anode is a combination of the current induced by the avalanche ions as they drift towards the cathode, and the response of a charge-sensitive preamplifier.

For events above ~ 30 primary electrons, which includes some of the calibrations used in this work, the event amplitude, defined as the integral of the pulse, is used as an estimator of the event’s energy. Additionally, for point-like energy depositions, the 10% to 90% risetime of the integrated pulse is proportional to the diffusion experienced by primary electrons. As this increases with the radial position of the event, selection cuts on the risetime are used to reject surface background events.

For events with fewer than ~ 10 primary electrons, the signals are processed [14] to obtain a series of delta impulses, each corresponding to the arrival of an ionization electron to the anodes, with varying amplitudes proportional to the size of each avalanche.

The relatively large longitudinal diffusion of the electrons in methane results in $\mathcal{O}(100\ \mu\text{s})$ spread in their arrival times. This allows for the identification of individual primary electrons in processed traces for low energy events, such as those generated by low-mass WIMP recoils. A peak-finding (PF) algorithm based on the ROOT TSpectrum Search method [15, 16] is applied to estimate the number of electrons present in the waveform, their arrival times, and avalanche size. The number of observed peaks, which is linked to deposited energy, constitutes the first parameter on which the present analysis is based. Although this is connected to the number of primary electrons generated in the event, a fraction of them may be lost in baseline noise fluctuations, or electrons arriving in close temporal proximity might not be resolvable. The second parameter is the time separation between the first and the last peak. This parameter is used to statistically discriminate contributions from different background sources.

The relative signal of the two readout channels is used as an event quality selection. Electron multiplication occurring near an anode induces also a smaller signal of opposite polarity to the other anodes, as expected by the Shockley-Ramo theorem [17, 18] and discussed in Ref. [19]. The absence of this cross-channel signal for an event localised at one anode suggests it did not originate from ionization electron amplification in the detector, and hence was removed (“anti-spikes cut”).

The overall principle of the analysis is based on the comparison of the time separation distributions for 2, 3, and 4 observed peaks in data, and the expected backgrounds and signal. Only events collected from the “Far” hemisphere, where the electric field is more homogeneous, are considered, defining the analysis fiducial volume. Following an α -decay on the surface of the detector, there is a transient increase in the rate of single-electron events. Therefore, events occurring within 5 s after every α -particle detection were also discarded. The collected

dataset is separated into two subsets: 23% is the “test data” on which the analysis is tuned, and the remaining 77% is “DM search data” on which the search is performed.

Extensive calibrations of the detector response were carried out for this physics campaign. A UV laser calibration system was implemented as described in Ref. [20], producing a photodiode-tagged source of photoelectrons from the inner surface of the SPC vessel. The laser is coupled to an optical fibre which is fed into the active volume of the SPC, the bare end of which is directed at the far hemisphere of the SPC, from which photoelectrons are extracted.

During data collection, the UV laser was operated at a high intensity to monitor changes in the detector response in real-time. This revealed that over the course of physics data collection, the detector gas gain was reduced by approximately 11%, due to deterioration of the gas quality during operation in sealed mode. This is modelled as a piece-wise linear function for the detector gain over time.

When operated at low intensity, the UV laser can induce a signal dominated by single photoelectron events, which is used to model the detector response. The electron avalanche multiplication is modelled with the Polya distribution [20–24] with shape parameter θ , scaled to the mean gain of the detector $\langle G \rangle$. During the physics campaign, approximately 1 hour of calibration with the UV laser was obtained for each day of data-taking. The obtained estimated of the θ parameter is $0.125_{-0.023}^{+0.026}$, indicating an approximately exponential distribution.

Additionally, the UV laser was used to determine the detector trigger efficiency. An emulation of the online trigger algorithm was applied to the laser calibration data, and it was found that $64_{-3}^{+4}\%$ of single-electron and as much as $93_{-1}^{+2}\%$ of double-electron events fulfill the trigger requirement. For multiple-electron events close to the anodes, the increased electron pile-up probability increases the trigger efficiency.

The performance of the PF method was also evaluated using laser data. On average, $62.5 \pm 0.3\%$ of single electrons fulfill the amplitude threshold for peak detection, with a small time dependence as the detector gain decreased during the campaign. The minimum time separation required for the PF method to distinguish two electrons was calibrated with double-peak laser data; the observed rate drops off for events with very short time separations, which was fit with an error function with a threshold of $8.2 \pm 0.4\ \mu\text{s}$. The PF parameters were chosen so as to minimize the probability of baseline noise generating a false peak, to avoid single-electron events being reconstructed as containing two peaks. A probability of 0.03% per search window was obtained, allowing this effect to be neglected. From these results, a model was developed to compute the probability that events with n primary electrons and expected diffusion time σ will be reconstructed as having k peaks. The resulting predictions for three and four-peak events were consistent with

the respective laser calibration data.

At the end of the physics campaign, ^{37}Ar was injected into the detector. Decaying via electron capture, ^{37}Ar produces low-energy electrons and X-rays uniformly throughout the detector volume. The dominant total energy depositions per event are 270 eV and 2.8 keV [25, 26] with smaller contributions from different decay paths and partially escaped decays [27].

This calibration data is used to measure *in situ* the overall energy response, including the mean avalanche gain of all six far-channel anodes. The ionization yield $W(E)$ of the detector for interactions induced by electrons and photons, collectively referred to as electronic recoils, is parametrized using the expression of Ref. [28], with free parameters U for the asymptote, and W_0 as the corresponding high energy limiting value. Independent measurements of W_0 and U were performed¹ and used as a prior for the present calibration, leading to a result of $W_0 = 30.0^{+0.14}_{-0.15}$ eV and $U = 15.70^{+0.52}_{-0.34}$ eV. The statistical dispersion of ionization is controlled by the Fano factor [29], whose value was obtained from the literature [30] as an exact number, given there were no uncertainties provided. This dispersion was modelled with a COM-Poisson distribution [31, 32]. Primary electron losses through attachment are parameterized using this calibration data by assuming a survival probability varying linearly with radial position.

The ^{37}Ar data was used to characterize electron diffusion as a function of radius, following an empirical relationship of $\sigma(r) = \sigma_{\text{max}}(r/r_{\text{max}})^\alpha$, with σ being the standard deviation of the electron arrival time, r the radius of the interaction, the subscript max indicating the value at the cathode surface ($\sigma_{\text{max}} = 123.5 \pm 1.1 \mu\text{s}$ for physics runs), and $\alpha = 3.05 \pm 0.15$. This diffusion model was combined with the PF performance model to generate Monte Carlo (MC) simulations of two, three, and four-peak events in ^{37}Ar data. The simulation was fine-tuned with the corresponding calibration data.

The detector response to nuclear recoils is affected by the ionization quenching factor (QF), defined as the ratio of ionization energies released by a nuclear and an electronic recoil of the same kinetic energy. Two independent measures of the QF for hydrogen atoms in CH_4 were used in this analysis: a) A NEWS-G measurement with the COMIMAC facility was performed between 2 and 13 keV [33]; and b) a QF curve was estimated from W-value measurements in the energy range 510 eV to several hundreds of keV [34]. The latter was conservatively scaled down by 15% to be in agreement with the COMIMAC measurement. Below 510 eV, the extrapolation $QF(E_K) = 0.428 + 0.224 \ln(E_K)$ was used based on the scaled W-value curve. This approach is conservative compared to an extrapolation based on the widely used Lindhard-model [35] (see Fig. 1).

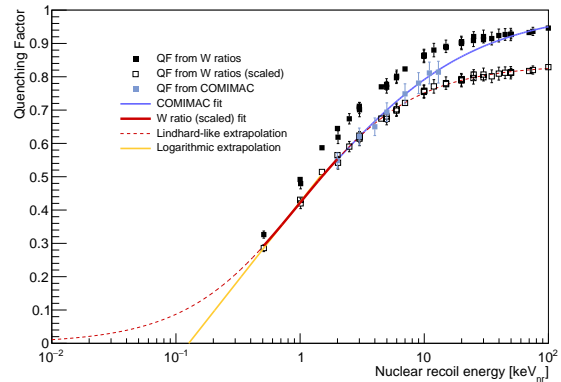


FIG. 1. Quenching factor used in this work. The curves used, from highest to lowest energies, are the COMIMAC measurement (lavender line [33], above 2 keV), scaled W-value ratios (red line [34], between 2 keV and 510 eV), and a logarithmic extrapolation (orange line, below 510 eV); the Lindhard-like extrapolation is shown for comparison (dotted red [35]).

The fiducial volume acceptance of the detector’s far channel for 2 through 15 electron events was determined as a function of their radial position using an MC electron drift simulation. COMSOL was used to model the electric field [36], and gas property data was obtained from MAGBOLTZ [37]. For example, 2-electron (15-electron) events originating from the cathode surface of the SPC have a $73.83 \pm 0.04\%$ ($64.72 \pm 0.05\%$) probability of fulfilling the fiducialization cut. The fiducialization efficiency was validated against ^{37}Ar calibration data. The efficiencies of the additional event selection requirements, were also estimated. The α -particle cut results in a 14% dead-time. The “anti-spikes” cut removes 95% of events not associated with an electron avalanche while keeping 77% of ionization electrons. Removing tagged laser calibration events reduces the effective runtime by 0.48%.

After applying the previous selection criteria, a rate of 403 mHz of single-peak events was observed in the test data, compared to only 6.5 and 1.1 mHz of two and three-peak events, respectively. In the absence of an explanation for such a high single-electron event rate, it was decided to keep only events with two or more peaks to calculate WIMP exclusion limits. The combined detection and selection cut efficiency for volume events with up to 15 electrons for the physics conditions of this work are shown in Tab. I.

After data quality requirements, the test data contained 6.5, 1.1, and 0.78 mHz of 2, 3, and 4-peak events, respectively. The corresponding time separation distributions were inconsistent with the expectation for events happening in the detector volume, implying the presence of backgrounds.

In preparation for fitting the data, the same MC simulations used for calibrations were adapted for WIMP recoils of different masses and three background sources, identifiable by their time separation distributions: con-

¹ Paper in preparation

Peaks	Primary Electrons													
	2	3	4	5	6	7	8	9	10	11	12	13	14	15
2	0.124	0.227	0.265	0.255	0.221	0.181	0.144	0.112	0.088	0.069	0.056	0.046	0.038	0.033
3	-	0.049	0.117	0.174	0.206	0.213	0.203	0.183	0.158	0.133	0.111	0.092	0.077	0.064
4	-	-	0.016	0.051	0.093	0.132	0.161	0.176	0.179	0.172	0.160	0.144	0.127	0.111
Total	0.124	0.276	0.400	0.480	0.522	0.527	0.509	0.472	0.426	0.375	0.327	0.283	0.243	0.210

TABLE I. Combined detection and selection efficiency for volume events, depending on the number of primary electrons.

taminants on the internal surface of the detector, particle interactions in the gas volume, and accidental coincidences.

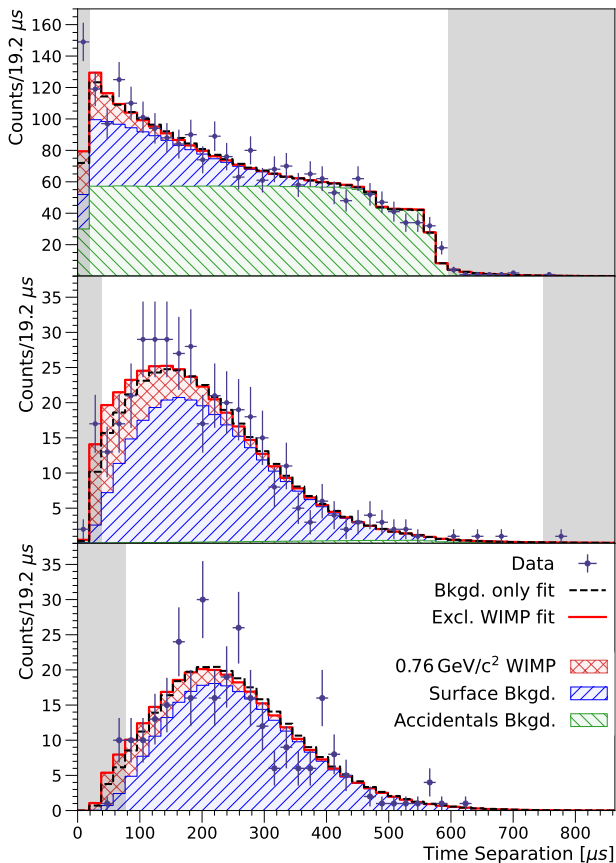


FIG. 2. Top to bottom: Fit (red line) of the time separation distribution of (respectively) 2, 3, and 4-peak DM search data (dark blue points), with the stacked contributions from surface (blue hashed) and accidental coincidence (green hashed) backgrounds, together with a $0.76 \text{ GeV}/c^2$ WIMP contribution (red hashed) fixed to the 90% C.L. excluded cross-section, $\sigma_{SDp} = 30.9 \text{ pb}$. The best background-only fit (black dashed line), including background volume events, is shown for comparison. The shaded grey areas cover the regions where simulations did not match calibrations, and so were not included in the fit.

For the WIMP elastic scattering recoil energy spectrum, the standard halo parametrization with $\rho_0 = 0.3 \text{ GeV}/c^2/\text{cm}^3$, $v_0 = 238 \text{ km/s}$, $v_{\text{Earth}} = 232 \text{ km/s}$, and

$v_{\text{esc}} = 544 \text{ km/s}$ [38–41] was used, together with the Helm form factor for the nuclear cross-section [42], which is nearly identical to 1. The binding energy of hydrogen to CH_3^+ [43] was subtracted from the recoil kinetic energy. The rate of WIMP events in the three categories was scaled by the WIMP–proton spin-dependent cross-section, σ_{SDp} , which is the parameter of interest.

For surface and volume backgrounds, an underlying energy distribution of the form $R(E) = A + Be^{-E/C}$ was assumed, where A , B , C are free parameters for surface and volume contributions separately. The A term represents backgrounds with a uniform energy distribution, such as from Compton interactions; the $Be^{-E/C}$ term is a generic parametrization for rising background rates at low energies, as observed in multiple DM direct detection experiments [44] including the previous NEWS-G detector [5]. For surface events, the large diffusion time made overlapping electrons less frequent. This, in turn, made the time separation distribution of surface events insensitive to the underlying energy distribution, modifying only the relative rates of observed 2, 3, and 4-peak events. Conversely, for volume events, their shorter diffusion time increased the frequency of overlaps and hence the proportion of events with higher number of electrons reconstructed as only having 2 to 4 peaks.

The last background considered was accidental coincidences of unrelated events within $523 \mu\text{s}$ of the trigger time or false positives of the PF method due to baseline noise fluctuations. These were modelled with an MC assuming a uniform time distribution of peaks within the search window, and corroborated by comparing with the distribution of 2, 3, or 4-peak events after an α -particle, when the increased single-electron event rate produced high rates of coincidences. The rates for each of 2, 3, and 4-peak coincident events were left as free independent parameters.

The 2, 3, and 4-peak data were jointly fit with these four components using the profile likelihood ratio (PLR) test statistic [45]. The fit results on the DM search data are shown in Table II, with an overall background rate of a few mHz. The main contributions were from surface contamination and accidental coincidences, with a smaller contribution from volume background events.

A constraint on the WIMP–proton spin-dependent cross section was obtained by profiling the likelihood ratio over the rates of the surface and accidental coincidence events; volume background events were fixed to

	2-peak	3-peak	4-peak
Accidental Coincidences	4.42 ± 0.30	0.02 ± 0.03	0.00 ± 0.01
Surface Background	1.43 ± 0.29	0.83 ± 0.08	0.73 ± 0.07
Volume Background	0.21 ± 0.12	0.15 ± 0.08	0.09 ± 0.05
0.76 GeV/c ² WIMP	0.28	0.19	0.11

TABLE II. Background rates in mHz obtained from background-only fit on the DM search data. Excluded contribution from 0.76 GeV/c² WIMP shown for comparison.

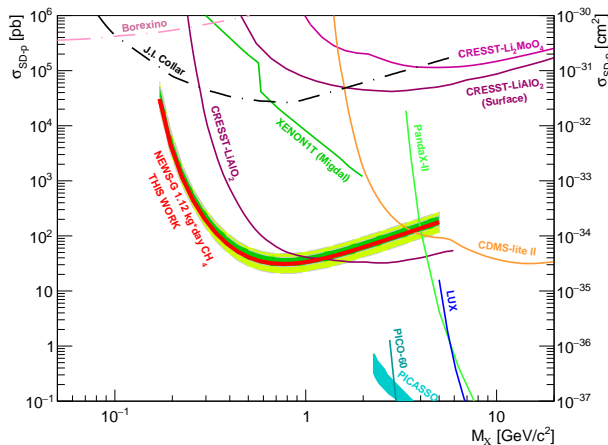


FIG. 3. Exclusion limit on the WIMP–proton spin-dependent cross section from this work (thick red line) and 1 and 2σ sensitivity bands (dark and light green shaded areas respectively). Upper limits from CDMS-lite [46], CRESST-III [47–49], LUX [50], PANDAX-II [51], XENON-1T (Migdal) [52], PICASSO [53], PICO-60 [54], J.I. Collar [55] and Borexino [56] are also shown.

zero due to their near-degeneracy with WIMP events. Pseudo datasets were simulated based on the best fit of the test data for various WIMP masses, with cross sections fixed to different values and scaled to the exposure of the DM search data. The distribution of the PLR from these datasets was used to obtain the threshold value of the test-statistic for the 90% confidence level (C.L.) cross-section exclusion limit. In Fig. 2, the fit result is shown for a WIMP with mass 0.76 GeV/c² and a $\sigma_{SD,p}$ fixed at 30.9 pb (excluded at 90% C.L.).

The resulting upper limit curve is shown in Fig. 3. Sys-

tematic uncertainties from the exposure or selection efficiencies were accounted for by taking their conservative values at 95% C.L., and were found to have a negligible effect. The effect of systematic uncertainties on the DM candidate-induced nuclear recoil ionization process was considered through variations of the W_0 and U parameters. Negligible effects were observed. The dominant systematic uncertainty was the choice of the QF extrapolation, where the nominal approach was replaced by assuming the QF becomes zero for energies below 510 eV. The curve in Fig. 3 shows the worst-case scenario among all considered combinations.

New constraints on spin-dependent DM interactions with protons are presented in the mass range 0.17 to 1.2 GeV/c², with a 90% confidence level cross section upper limit of 30.9 pb for a mass of 0.76 GeV/c².

ACKNOWLEDGMENTS

The help of the technical staff of the Laboratoire Souterrain de Modane is gratefully acknowledged. This research was undertaken, in part, thanks to funding from the Canada Excellence Research Chairs Program, the Canada Foundation for Innovation, the Arthur B. McDonald Canadian Astroparticle Physics Research Institute, Canada, the French National Research Agency (ANR-15-CE31-0008), and the Natural Sciences and Engineering Research Council of Canada. This project has received support from the European Union’s Horizon 2020 research and innovation programme under grant agreements No. 841261 (DarkSphere), No. 845168 (neutronSPHERE), and No. 101026519 (GaGARin). Support from the U.K. Research and Innovation — Science and Technology Facilities Council (UKRI-STFC), through grants No. ST/V006339/1, No. ST/S000860/1, No. ST/W000652/1, No. ST/X005976/1, and No. ST/X508913/1, the UKRI Horizon Europe Underwriting scheme (GA101066657/Je-S EP/X022773/1), and the Royal Society International Exchanges Scheme (IES\R3\170121) is acknowledged. Support by the Deutsche Forschungsgemeinschaft (DFG, German Research Foundation) under Germany’s Excellence Strategy — EXC 2121 “Quantum Universe” — 390833306 is acknowledged.

- [1] D. Clowe, M. Bradač, A. H. Gonzalez, M. Markevitch, S. W. Randall, C. Jones, and D. Zaritsky, A direct empirical proof of the existence of dark matter, *The Astrophysical Journal* **648**, L109 (2006).
- [2] P. A. R. Ade *et al.* (Planck Collaboration), Planck 2015 results. XIII. Cosmological parameters, *A&A* **594**, A13 (2016), [arXiv:1502.01589 \[astro-ph.CO\]](https://arxiv.org/abs/1502.01589).
- [3] D. Akerib *et al.*, *Snowmass2021 cosmic frontier dark mat-*

- ter direct detection to the neutrino fog* (2022).
- [4] C. Patrignani *et al.* (Particle Data Group), Review of Particle Physics, *Chin. Phys.* **C40**, 10.1088/1674-1137/40/10/100001 (2016).
- [5] Q. Arnaud *et al.* (NEWS-G Collaboration), First results from the NEWS-G direct dark matter search experiment at the LSM, *Astropart. Phys.* **97**, 54 (2018).
- [6] L. Balogh *et al.* (NEWS-G collaboration), The NEWS-G

- detector at SNOLAB, *JINST* **18** (02), T02005.
- [7] L. Balogh *et al.*, Copper electroplating for background suppression in the news-g experiment, *Nucl. Instrum. Methods Phys. Res., Sect. A* **988**, 164844 (2021).
- [8] A. Giganon, I. Giomataris, M. Gros, I. Katsioulas, X. F. Navick, G. Tsiledakis, I. Savvidis, A. Dastgheibifard, and A. Brossard, A multiball read-out for the spherical proportional counter, *JINST* **12** (12), P12031, [arXiv:1707.09254](https://arxiv.org/abs/1707.09254) [physics.ins-det].
- [9] I. Giomataris *et al.*, A resistive ACHINOS multi-anode structure with DLC coating for spherical proportional counters, *JINST* **15** (11), P11023.
- [10] R. Essig *et al.*, Dark sectors and new, light, weakly-coupled particles, (2013), [arXiv:1311.0029](https://arxiv.org/abs/1311.0029).
- [11] Alexander, J. and others, Dark Sectors 2016 Workshop: Community Report (2016) [arXiv:1608.08632](https://arxiv.org/abs/1608.08632).
- [12] K. M. Zurek, Asymmetric Dark Matter: Theories, signatures, and constraints, *Phys. Rep.* **537**, 91 (2014), Asymmetric Dark Matter: Theories, signatures, and constraints.
- [13] K. Petraki and R. Volkas, Review of asymmetric dark matter, *Int. J. Mod. Phys. A* **28**, 1330028 (2013).
- [14] F. A. Vazquez de Sola Fernandez, *Solar KK axion search with NEWS-G*, Ph.D. thesis, Queen's University (2020).
- [15] R. Brun and R. F., Root - an object oriented data analysis framework, *Nucl. Inst. & Meth. in Phys. Res. A* **389**, 81 (1997).
- [16] M. Morhac, [TSpectrum class reference](https://www.root-project.org/ROOT/html/TSpectrum-class-reference.html).
- [17] W. Shockley, Currents to conductors induced by a moving point charge, *Journal of Applied Physics* **9**, 635 (1938), <https://doi.org/10.1063/1.1710367>.
- [18] S. Ramo, Currents induced by electron motion, *Proceedings of the IRE* **27**, 584 (1939).
- [19] I. Katsioulas, P. Knights, I. Manthos, J. Matthews, T. Neep, K. Nikolopoulos, and R. Ward, ACHINOS: a multi-anode read-out for position reconstruction and tracking with spherical proportional counters, *JINST* **17** (08), C08025, [arXiv:2211.11569](https://arxiv.org/abs/2211.11569) [physics.ins-det].
- [20] Q. Arnaud *et al.* (NEWS-G Collaboration), Precision laser-based measurements of the single electron response of spherical proportional counters for the NEWS-G light dark matter search experiment, *Phys. Rev. D* **99**, 102003 (2019).
- [21] J. Derré, Y. Giomataris, P. Rebougeard, H. Zaccane, J. Perroud, and G. Charpak, Fast signals and single electron detection with a MICROMEAS photodetector, *Nucl. Instrum. Methods Phys. Res., Sect. A* **449**, 314 (2000).
- [22] T. Zerguerras, B. Genolini, V. Lepeltier, J. Peyré, J. Pouthas, and P. Rosier, Single-electron response and energy resolution of a Micromegas detector, *Nucl. Instrum. Methods Phys. Res., Sect. A* **608**, 397 (2009).
- [23] M. Kobayashi *et al.*, A novel technique for the measurement of the avalanche fluctuation of gaseous detectors, *Nucl. Instrum. Methods Phys. Res., Sect. A* **845**, 236 (2017).
- [24] R. Bellazzini *et al.*, Imaging with the invisible light, *Nucl. Instrum. Methods Phys. Res., Sect. A* **581**, 246 (2007).
- [25] Barsanov, V.I. and others, Artificial neutrino source based on the ^{37}Ar isotope, *Phys. Atom. Nucl.* **70**, 300 (2007).
- [26] F. G. Kelly, Q. Arnaud, A. E. Brossard, E. C. Corcoran, D. Durnford, G. Gerbier, A. Fauschou, J. M. McDonald, T. Mumby, and P. Samuleev, The production of Ar-37 using a thermal neutron reactor flux, *J. Radioanal. Nucl. Ch.* **318**, 279 (2018).
- [27] P. Agnes *et al.* (DarkSide Collaboration), Calibration of the liquid argon ionization response to low energy electronic and nuclear recoils with DarkSide-50, *Phys. Rev. D* **104**, 082005 (2021).
- [28] M. Inokuti, Ionization Yields in Gases under Electron Irradiation, *Radiat. Res.* **64**, 6 (1975).
- [29] U. Fano, Ionization yield of radiations. II. The fluctuations of the number of ions, *Phys. Rev.* **72**, 26 (1947).
- [30] B. Grosswendt and E. Waibel, Statistical ionisation yield fluctuations and determination of spatial ionisation and energy absorption for low energy electrons, *Radiat. Prot. Dos.* **13**, 95 (1985).
- [31] K. Sellers, S. Borle, and G. Shmueli, The COM-Poisson model for count data: A survey of methods and applications, *Appl. Stoch. Models Bus. Ind.* **28**, 104 (2011).
- [32] D. Durnford, Q. Arnaud, and G. Gerbier, Novel approach to assess the impact of the Fano factor on the sensitivity of low-mass dark matter experiments, *Phys. Rev. D* **98**, 103013 (2018).
- [33] L. Balogh *et al.* (NEWS-G collaboration), Measurements of the ionization efficiency of protons in methane, *Eur. Phys. J. C* **82**, 1114 (2022), [arXiv:2201.09566](https://arxiv.org/abs/2201.09566) [physics.ins-det].
- [34] I. Katsioulas, P. Knights, and K. Nikolopoulos, Ionisation quenching factors from W-values in pure gases for rare event searches, *Astropart. Phys.* **141**, 102707 (2022).
- [35] J. Lindhard, V. Nielsen, M. Scharff, and P. V. Thomsen, Integral equations governing radiation effects. (notes on atomic collisions, III), *Kgl. Danske Videnskab., Selskab. Mat. Fys. Medd.* **33**, (1963).
- [36] COMSOL Multiphysics, Introduction to COMSOL multiphysics®, COMSOL Multiphysics, Burlington, MA, accessed Feb 9, 2018 (1998).
- [37] S. F. Biagi, Monte Carlo simulation of electron drift and diffusion in counting gases under the influence of electric and magnetic fields, *Nucl. Instrum. Methods Phys. Res., Sect. A* **421**, 234 (1999).
- [38] M. C. Smith *et al.*, The RAVE survey: constraining the local Galactic escape speed, *Mon. Not. R. Astron. Soc.* **379**, 755 (2007).
- [39] D. Cerdeño and A. Green, Direct detection of WIMPs, in *Particle Dark Matter: Observations, Models and Searches*, edited by G. Bertone (Cambridge University Press, Cambridge, UK, 2010) p. 347.
- [40] R. Schnee, Introduction to dark matter experiments, *Proc. TASI09*, 775 (2011).
- [41] Baxter, D. and others, Recommended conventions for reporting results from direct dark matter searches, *Eur. Phys. J. C* **81**, 907 (2021).
- [42] J. Lewin and P. Smith, Review of mathematics, numerical factors, and corrections for dark matter experiments based on elastic nuclear recoil, *Astropart. Phys.* **6**, 87 (1996).
- [43] B. Darwent, [Bond dissociation energies in simple molecules](https://www.scribd.com/document/38111111/Bond-dissociation-energies-in-simple-molecules) (1970).
- [44] P. Adari *et al.*, EXCESS workshop: Descriptions of rising low-energy spectra, *SciPost Phys. Proc.*, 001 (2022).
- [45] Cowan, G. and Cranmer, K. and Gross, E. and Vitells, O., Asymptotic formulae for likelihood-based tests of new physics, *Eur. Phys. J. C.* **71**, 1554 (2011).
- [46] R. Agnese *et al.* (SuperCDMS Collaboration), Low-mass dark matter search with CDMSlite, *Phys. Rev. D* **97**,

- 022002 (2018).
- [47] A. H. Abdelhameed *et al.* (CRESST collaboration), First results on sub-GeV spin-dependent dark matter interactions with ${}^7\text{Li}$, *Eur. Phys. J. C* **79**, 630 (2019), [arXiv:1902.07587 \[astro-ph.IM\]](#).
- [48] G. Angloher *et al.* (CRESST collaboration), Probing spin-dependent dark matter interactions with ${}^6\text{Li}$, *Eur. Phys. J. C* **82**, 207 (2022), [arXiv:2201.03863 \[physics.ins-det\]](#).
- [49] G. Angloher *et al.* (CRESST collaboration), Testing spin-dependent dark matter interactions with lithium aluminate targets in CRESST-III, *Phys. Rev. D* **106**, 092008 (2022), [arXiv:2207.07640 \[astro-ph.CO\]](#).
- [50] D. S. Akerib *et al.* (LUX Collaboration), Limits on spin-dependent WIMP-nucleon cross section obtained from the complete LUX exposure, *Phys. Rev. Lett.* **118**, 251302 (2017).
- [51] J. Xia *et al.*, PandaX-II constraints on spin-dependent WIMP-nucleon effective interactions, *Physics Letters B* **792**, 193 (2019).
- [52] E. Aprile *et al.* (XENON Collaboration), Search for light dark matter interactions enhanced by the Migdal effect or Bremsstrahlung in XENON1T, *Phys. Rev. Lett.* **123**, 241803 (2019).
- [53] E. Behnke *et al.*, Final results of the PICASSO dark matter search experiment, *Astroparticle Physics* **90**, 85 (2017).
- [54] C. Amole *et al.* (PICO Collaboration), Dark matter search results from the complete exposure of the PICO-60 C_3F_8 bubble chamber, *Phys. Rev. D* **100**, 022001 (2019).
- [55] J. I. Collar, Search for a nonrelativistic component in the spectrum of cosmic rays at Earth, *Phys. Rev. D* **98**, 023005 (2018).
- [56] T. Bringmann and M. Pospelov, Novel direct detection constraints on light dark matter, *Phys. Rev. Lett.* **122**, 171801 (2019).